COMPARATIVE ASSESSMENT OF MULTI-TEMPORAL INSAR TECHNIQUES FOR GENERATION OF DISPLACEMENT MAPS: A CASE STUDY FOR BUCHAREST AREA

Carmen PATRASCU[1], Anca Andreea POPESCU[2], Mihai DATCU[3]

This paper presents a comparative assessment of Synthetic Aperture Radar interferometric techniques (InSAR) that allow the detection of deformation models along the line-of-sight of the radar. Given the susceptibility of these methods to several limitations that act as noise effects in the interferograms, known as decorrelation phenomena, multi-temporal InSAR techniques have been used for the exploiting of phase information acquired over long time intervals.

Keywords: Synthetic Aperture Radar (SAR), SAR Interferometry (InSAR), Permanent Scatterers (PS), Small BAseline Subsets (SBAS)

1. Introduction

Differential InSAR (DInSAR) is a special processing technique that enables the combination of the phase information of at least two complex images acquired over the same area at simultaneous or different times for several applications. An important feature of DInSAR is the fact that topographic contributions to the resulting phase have been removed from the final results, thus allowing the extraction of linear deformations along the system's line of sight with millimetric accuracy [1][2]. These techniques are mainly used for extracting earth deformation patterns, with one of the most important application being the computation of digital elevation models (DEM) corresponding to the imaged scene [3]. Other applications include measuring the effects of a large series of ground deformation phenomena, such as: deformation induced by volcanic activity [4], co-seismic and post-seismic motions [5], mining and groundwater induced deformation [6][1], or measurement of the soil moisture [2]. However, the number of usable interferometric pairs, which has to range in the tens domain,

[1]PhD Student, Research Centre for Spatial Information – CEOSpaceTech, University POLITEHNICA of Bucharest, e-mail: cpatrascu@ceospacetech.pub.ro

[2] Associate Professor, Research Centre for Spatial Information – CEOSpaceTech, University POLITEHNICA of Bucharest, e-mail: apopescu@ceospacetech.pub.ro

[3] Professor, Research Centre for Spatial Information – CEOSpaceTech, University POLITEHNICA of Bucharest, German Aerospace Center (DLR – Oberpfaffenhofen), e-mail: mihai.datcu@dlr.de

is limited by noise like effects noticeable in the computed interferograms, known as decorrelation phenomena [7]. Apart from these, other limitations are mainly due to cycle ambiguity problems caused by the necessity of both SBAS and PS techniques for phase unwrapping [8] and extraction of atmospheric induced artifacts.

Multi-temporal InSAR techniques are extensions of conventional InSAR methods that aim at addressing problems caused by decorrelation effects and atmospheric delay. These techniques involve the simultaneous processing of multiple SAR acquisitions of the same area extended over large periods of time to allow for the correction of the uncorrelated phase noise terms, reducing errors associated with deformation elements. At this moment, these techniques fall into two main categories: permanent scatterer techniques (PSInSAR) [11-13] and small baseline subset algorithms (SBAS) [14][15]. These methods try to overcome limitations induced by large baseline values by using points characterized by long-term phase coherence, known as persistent (PS) or distributed (DS) scatterers.

In non-urban areas the incidence of such points is low, due to the reduced number of scatterers with sufficiently high coherence levels. For this reason, a method to improve the coherence estimates must be found. A straightforward solution is given by multi-looking techniques, which perform filtering of the interferometric phase by computing a weighted average of pixels located in a neighborhood [9]. An adaptive approach is proposed, which selects statistically homogeneous pixels by analyzing the temporal distribution of the amplitude levels in a goodness-of-fit approach. The resulting phase estimates are filtered for non-uniform contributions (APS), allowing for the extraction of deformation profiles for the analyzed area.

This article aims at performing a complete analysis of the millimetric deformations which affect the area of Bucharest using both PSInSAR and SBAS techniques. A comparison of the results will be performed. The proposed methodology has been applied on a set of 32 TerraSAR-X images, acquired over the South-Eastern area of Romania. The image stack covers a period of 16 months, from July 2011, to December 2012.

The remainder of this paper is organized as follows. Section 2 presents the methods used by the authors to extract point-wise deformation histories using the PSInSAR and SBAS approaches. The adaptive phase filtering algorithm will be described. Experimental results (Section 3) and the conclusions (Section 4) will contribute to the assessment of both methods' performances.

2. Methodology for extraction of deformation maps

In order to obtain an estimate of the displacement rates in the test area, we employ a processing workflow based on the functionality of the GAMMA interferometric processor [10]. Starting from a set of N available SLC images, M differential interferograms are generated using either a single reference (PSInSAR) or a SB constraint (SBAS). The results of this step are adaptively filtered and used to extract deformation histories for targets located in the analyzed area. The main processing steps are detailed in the following sections.

2.1. Persistent Scatterer Interferometry (PSInSAR)

In the case of differential interferometry, the resulting phase represents the phase difference between two considered acquisitions, from which the influence of the topography has been removed. However, if multiple acquisitions are considered, the phase of each pixel does not only change to the difference in the relative position between the target and the satellite, but also due to a temporal evolution of the target, as well as influence in the atmospheric term, especially for long observation intervals. Hence, the final estimate of the phase (ϕ_{i}) will comprise information about the acquisition geometry ($\phi_{\mathrm{R,i}}$), terrain motion ($\phi_{\mathrm{motion,i}}$), scattering properties of the imaged target ($\phi_{\mathrm{A,i}}$) and the atmospheric influence ($\phi_{\mathrm{APS,i}}$), as seen in Eq. (1).

$$\phi_i(p) = \phi_{R,i}(p) + \phi_{motion,i}(p) + \phi_{A,i}(p) + \phi_{APS,i}(p) \tag{1}$$

The persistent scatterer technique was first described in [11], [12]. The main goal of this approach is to overcome limitations imposed by the de-correlation phenomena and atmospheric induced limitations affecting conventional DInSAR systems, to compute deformation time series in the form of displacement maps [13]. The motivation behind this approach is that, in the case of methods based on the identification of stable targets, it is considered that only one scatterer in the resolution cell dominates the backscattered signal. Hence, a network of such scatterer-dominant pixels may be used to extract information signatures from interferograms that have been severely compromised by de-correlation effects.

Despite several terms influencing the phase of the final phase value corresponding to each interferometric acquisition, the amplitude values of the complex data are virtually insensitive to those variations, rendering amplitude statistics analysis a robust method for the extraction of stable targets. In the case of PS, we are interested in finding pixels characterized by high values of the SNR. Hence, the phase dispersion can be analyzed based on the dispersion of the amplitude values, as seen in Eq. (2).

$$\sigma_v \cong \frac{\sigma_A}{m_A} = D_A \tag{2}$$

where m_A and σ_A are the first and second moments of the amplitude computed in a neighborhood. The amplitude dispersion index offers information with respect to phase stability, and PS candidates are selected by thresholding ($D_A \leq 0.25$).

Important advantages of this processing method are the short time required for the analysis, as well as no resolution loss. However, its accuracy depends on the size of the image stack, used to estimate the statistical properties of the amplitude.

2.2. Small BAseline Subset Algorithm (SBAS)

If all scatterers have comparable strengths, then the interferometric phase is randomly distributed in the $[-\pi; +\pi]$ interval and the interferometric signal can be improved by averaging the signal from adjacent resolution cells. Under this assumption, the random contribution due to the movement of the scatterers cancel out and the results only account for the average motion of the resolution elements. This was originally the basis of the SBAS method [14].

Considering a series of $N+1$ images acquired over the same area at consecutive times $(t_0, \dots, t_N)$, a number of M unwrapped interferograms can be computed. Moreover, we assume that each image can interfere with at least another image under the baseline restriction considered, which implies that each small baseline (SB) subset has a minimum of two acquisitions.

If we assume that the images are chronologically ordered (i.e. the master image was acquired before the slave), the deformation values associated with the considered pixel can be obtained using the matrix representation in Eq. (3).

$$\delta\phi_j = \phi(t_{IE_j}) - \phi(t_{IS_j}) \Rightarrow A\phi = \delta\phi, \text{ for } i = \overline{1, M} \tag{3}$$

where A is an incidence-like matrix directly related to the interferograms generated from the available data and ϕ is the interferometric phase of the master (*IE*) and slave (*IS*) images .

In order to invert the system in Eq. (3), the Singular Value Decomposition (SVD) algorithm is employed [15]. This algorithm links the independent SAR acquisition data sets generated under the SB constraint. A direct advantage of this approach is the ability to include in the processing interferometric pairs which would otherwise be separated by large baselines and therefore not suitable for other processing methodologies.

Following this step, the phase estimate associated with the unknown deformation values can be extracted in an LS sense, as seen in Eq. (4).

$$\hat{\phi} = \sum_{i=1}^{N-L+1} \frac{\delta\phi^T u_i}{\sigma_i} v_i \tag{4}$$

where we define L as the number of generated subsets, and u_i and v_i are the column vectors of the U and V matrices resulting from the SVD decomposition. At this point, we can manipulate Eq. (4) and replace the unknowns with the mean velocity between time acquisitions, generating a physically sound solution.

The main purpose of the SBAS algorithm is to minimize the effects of spatial de-correlation and DEM errors. An important advantage of this method is the increase in the temporal sampling rate, due to the usage of all acquisitions in the subsets.

2.3. Adaptive Phase Improvement based on Amplitude Statistics

Long term monitoring of critical infrastructure is usually performed using coherent multi-temporal InSAR techniques, such as PSInSAR and SBAS. These methods use points that exhibit long term phase coherence, known as persistent and distributed scatterers, to overcome limitations induced by long time intervals between acquisitions. Given the relatively low incidence of such elements, especially in non-urban areas, a good estimation of the phase values and, consequently, complex correlation, is mandatory to achieve accurate results [16]. Authors in [10] have proved that using the backscattered amplitude statistics represents an efficient method to adaptively extract regions of homogeneous pixels, leading to the preservation of phase signatures in the analyzed region.

Traditional multi-looking methods use sliding windows with rectangular form and perform a weighted averaging of the neighboring complex pixels, under the hypothesis of statistical homogeneity [17]. However, in the case of high resolution data, this hypothesis is extremely short lived when increasing the size of the neighborhood given the different scattering phenomenology of the analyzed targets.

Due to different shapes and properties of objects in high resolution images, elements with similar statistical properties can be several pixels away. The concept behind the proposed approach is to average each considered element only with such pixels that are adaptively selected based on the similarities of their scattering properties.

We employ the Anderson-Darling (AD) test to perform a statistical analysis of the complex data in a goodness-of-fit approach, by temporally sampling the image stack using stationary time intervals. The AD method gives more weight to the tail of the distribution [18], leading to a better performance in the case of radar applications, where the information in the tail plays an important rose due to the influence it has on higher statistic order moments. The test statistic is defined in Eq. (5).

$$A^2_{M,M} = \frac{M}{2}\sum_{x\in x_p,x_q}\frac{(\hat{F}_p(x)-\hat{F}_q(x))^2}{\hat{F}_{pq}(x)(1-\hat{F}_{pq}(x))} \tag{4}$$

where $\hat{F}_{k,k=p,q}(x)$ represents the empirical cumulative distribution function (ECDF) of the analyzed pixel and all neighboring pixels from the patch (p), while $\hat{F}_{pq}(x)$ is the ECDF of the new population obtained by merging and ordering independent data sets corresponding to the current and tested pixels (q) into one set. The threshold used for processing was selecting empirically. Processing was

carried out with a number of *L=200* looks. An example of statistically homogeneous pixels selected based on the AD approach is presented in Fig. 1.

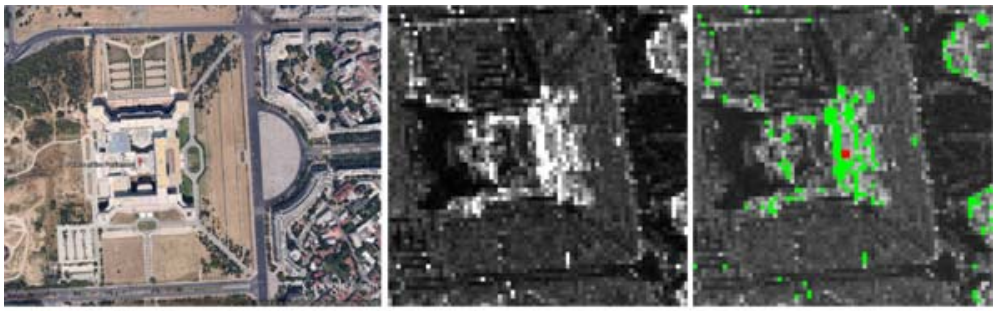

Fig.1. (a) Google Earth (© Google Inc.) image of the Palace of Parliament; (b) Amplitude image of a TerraSAR-X acquisition corresponding to the same area; (c) Goodness-of-fit for homogeneous area identification: the statistically homogeneous pixels selected based on the AD test are shown in green for the analyzed pixel (marked in red).

The influence of the image stack size is minimized by the dynamic expansion of the population associated to each identified homogeneous area. This way, the statistical test will be performed between the temporal PDF of each considered pixel and the PDF of the entire population included in one region, leading to increased confidence levels in the analysis, given the size of the population. Furthermore, the optimal size of the sliding windows included in the processing has been computed by employing the rate distortion theory and analyzing the level of variability in the neighborhood.

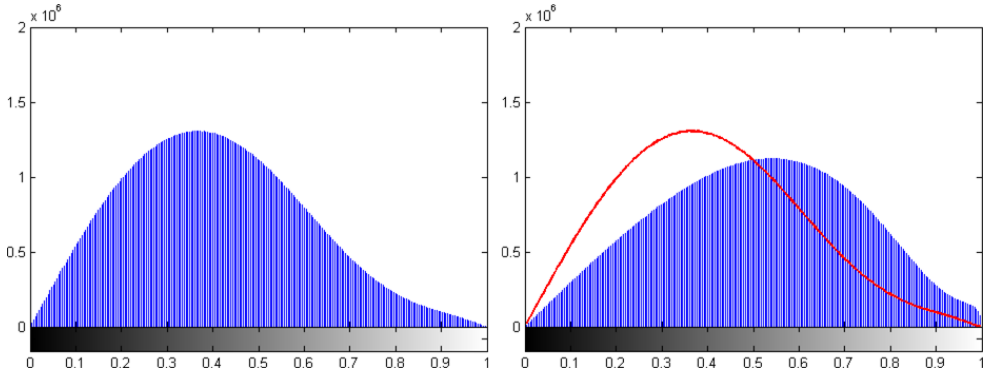

Fig.2. Coherence histograms for the initial (left) and adaptively filtered (right) differential interferograms. The result corresponds to the (07.04.2012 – 18.07.2011) image pair. The histogram before the adaptive filtering is superimposed in red. An increase of 3.53% in the total number of pixels selected for further processing ($\gamma > 0.4$) is observed.

The effects of the adaptive filtering method are presented using the estimated coherence of the interferometric phase. Figure 2 shows the histogram of coherence estimates before and after the ML operation. The results correspond to the (07.04.2012 – 18.07.2011) image pair. To measure the improvement effected by the usage of this algorithm, we compute the number of pixels included in the following processing steps ($\gamma > 0.4$). An increase of 3.6% in the overall number of unwrapped pixels has been observed.

3. Experimental Setup and Results

The proposed methodology has been tested on a dataset consisting of 32 SLC StripMap TerraSAR-X images, acquired over the area of Bucharest, Romania. The data spans a 16 months' temporal interval, between July 2011 and December 2012. All acquisitions are characterized by a descending orbit and HH polarization.

In the case of the PSInSAR technique, the image stack was processed based on a single acquisition, namely the image on 07.04.2012. Two criteria were employed in this selection: minimization of the perpendicular baseline values and acquisition date near the center of the studied temporal interval. For the SBAS method, a number of *M=134* differential interferograms are generated under the imposed SB constraint ($B_{perp} \leq 200$m).

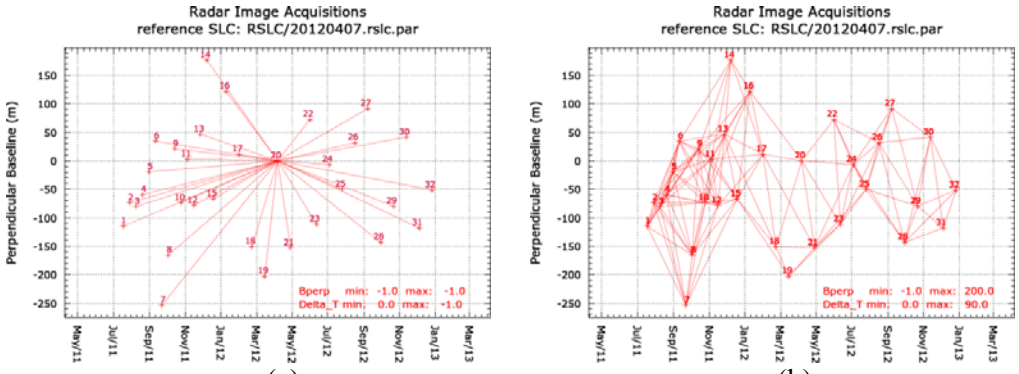

(a) (b)

Fig.3. Distribution of the spatial and temporal baselines computed using the PSInSAR (a) and SBAS (b) methods. As can be observed, the values of the perpendicular baselines are kept small, the absolute maximal value being of 250m for PSInSAR and 89.5m for the SBAS algorithm

The baseline distributions' graphs are presented in Fig. 3. As can be observed, both methods lead to the generation of small baseline values. In the case of PSInSAR method, the absolute maximal value is of 250m, with a medium

value of 46.7m. For the SBAS algorithm, the average value of the perpendicular component is 89.5m, while the temporal value is 99 days.

Following this step, the PSInSAR method is used to extract an initial set of persistent scatterer candidates, using the intensity variation of image targets. Following this process, a mask corresponding to the PSC locations is created and used to generate the differential interferograms. At this point, a multi-looking algorithm with L=200 looks is applied for the adaptive filtering of the interferometric phase computed for both algorithms.

In the case of PSInSAR method, the final displacement rates are computed after an iterative process which improves the baseline estimates and extracts the influence of the APS. For the SBAS method, an SVD inversion is applied to information extracted from the data itself, to link the independent image subsets generated under the SB subsets. Following an additional integration step, displacement histories can be extracted for all points included in the processing.

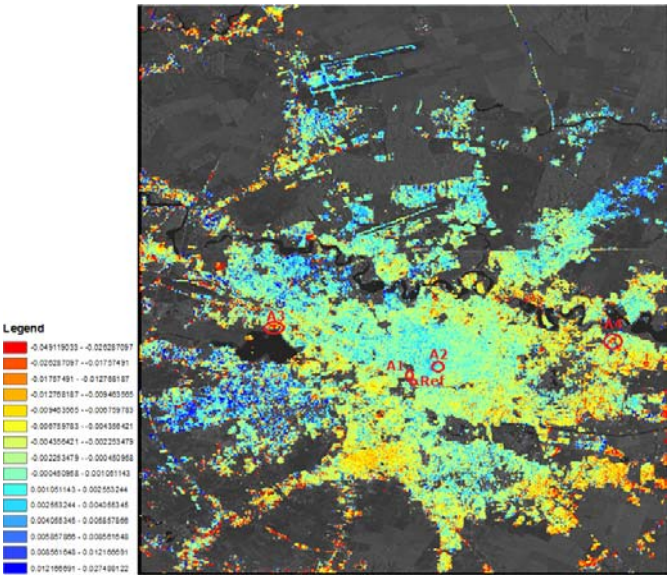

Fig.4. Average displacement rates [meters/year] for the TerraSAR-X image stack, corresponding to the Bucharest area.

A preliminary analysis of the average displacement rates [meters/year] for the TerraSAR-X image stack, allows us to identify three interest regions characterized by significant deformation phenomena (A1-A3 in Fig.4), with respect to a reference point (marked "Ref" in Fig.4). We present for comparison deformation histories for the A2 and A4 areas. The following conclusions were drawn with respect to the presented points:

- A1: historical building (built in 1906) corresponding to the former Bucharest City Hall premises (until 2010). It can be observed that an accentuated

deformation phenomenon is present in the results. Currently, the building is closed for consolidation work;

- A2: office building with 19 floors, completed in 2006. This building is located in the proximity of a historic monument. It is important to note that at the moment of the construction there was a strong controversy about its stability;
- A3: small area in the Northern part of the Morii Lake. A constant small deformation rate corresponding to the subsidence motion has been observed in the area in two more datasets (ASAR, ERS). The area consist of apartment buildings and is located in the vicinity of the Granmetal Industrial platform;
- A4: Esplanada Commercial Center. Strong subsidence was observed in the area following the processing of the TerraSAR-X dataset. This region is situated in the Eastern part of Bucharest and houses a new retail space comprising of a supermarket and shopping center.

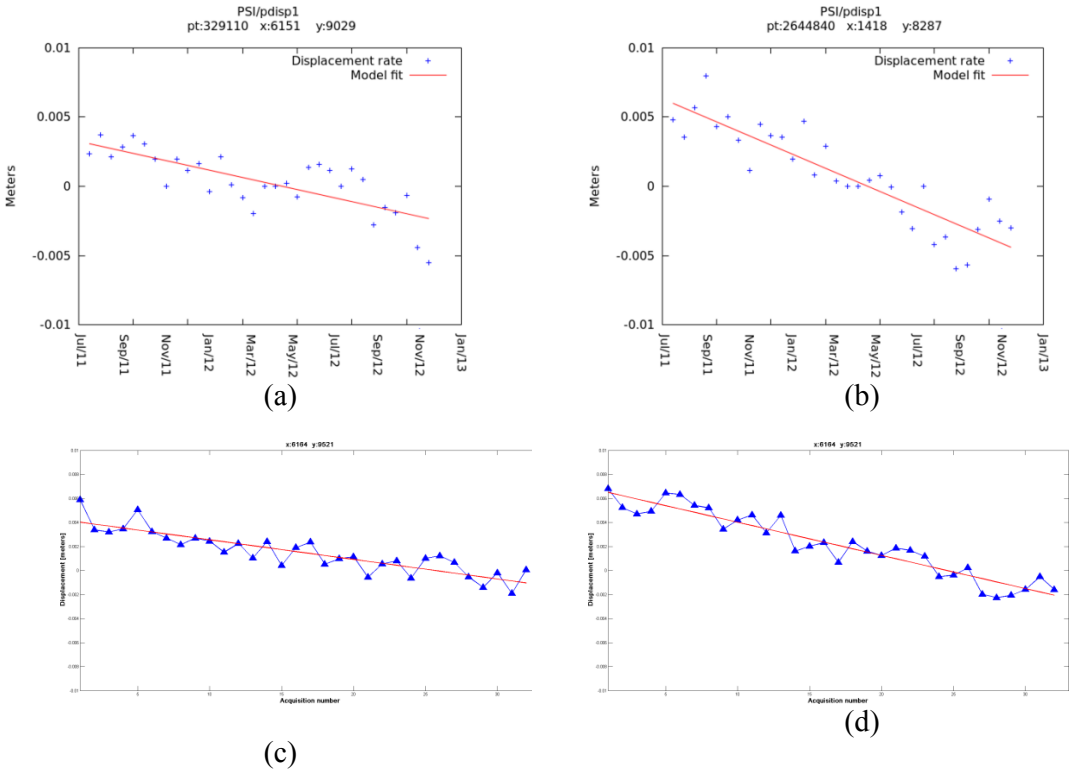

Fig.5. Deformation histories for points in the A1 and A4 interest regions extracted with the PSInSAR (a,b) and SBAS (c,d) methods; (a) A1 region, ($\overline{\sigma_{\text{phase}}} = 0.8$ rad); (b) A4 region, ($\overline{\sigma_{\text{phase}}} = 0.76$rad); (c) A1 region, ($\overline{\sigma_{\text{est}}} = 0.0023$ m); (d) A4 region, ($\overline{\sigma_{\text{est}}} = 0.0027$ m).

Displacement rates for the points extracted using the PS approach from the interest region are presented in Fig.5. Using the small baseline technique, we have extracted several areas affected by this phenomenon. The upper graphs show the displacement rate measured using the PSInSAR method, and the linear regression model superimposed in red. The second line depicts the results from the SBAS method, with the graphics representing deformation profiles.

In the absence of an external validation method in the form of ground truth measurements (GPS, leveling), the quality of the displacement estimates was assessed by means of the estimate variance, computed using equally sized sets defined by the coordinates of the identified PS. In this case, a significant narrowing of 3% is observed. Moreover, average displacement rates computed by the PSInSAR and SBAS algorithms show a very high correlation coefficient (ρ = 0.9438). This result proves similar displacement trends and values in both methods.

4. Conclusions

This paper presents a complete multi-temporal analysis methodology for the monitoring of small coherent displacements in the area of Bucharest, Romania, based on TerraSAR-X data acquired over a period of 16 months. We extract point-wise displacement trends using a persistent scatterer methodology and imposing a SB constraint on the perpendicular values of the baselines.

The processing workflow incorporates an improvement of the coherence estimates performed by employing an adaptive phase filtering algorithm which selects statistically homogeneous areas based on the amplitude temporal statistics of the SLC data, leading to the conservation of interferometric phase information of the analyzed targets.

In general, the quality of multi-temporal InSAR techniques is very difficult to assess without the existence of a priori knowledge about the deformation in the area. Given the absence of ground truth information, we propose the assessment of the displacement estimates by means of the estimate variance. This result shows a significant narrowing for equally sized sample sets. The estimated displacement rates for both methods are highly correlated, proving the similarity of displacement trends and values.

A small deformation trend in the W-E direction was detected and extracted. The displacement histories are in accordance with results published following independent studies on ENVISAT and TerraSAR-X data for the area [19].

Acknowledgement

This work was supported by the Romanian Sectoral Operational Programme Human Resources Development 2007-2013 of the Ministry of European Funds through the Financial Agreements POSDRU/107/1.5/S/76903 and POSDRU/159/1.5/S/132395. This work was supported by a grant of the Romanian National Authority for Scientific Research, CNCS – UEFISCDI, project number PN-II-ID-PCE-2011-3-1027.

The work has been funded by: Sectoral Operational Programme Human Resources Development 2007-2013 of the Romanian Ministry of Labour, Family and Social Protection through the Financial Agreement POSDRU/159/1.5/S/ 132395.

R E F E R E N C E S

[1] *L. Gong, J. Zhang, Z. Chang, Z. Li, and Q. Guo, M. Ivan,* "Measuring Mining Induced Subsidence with", Proceedings of IEEE International Geoscience and Remote Sensing Symposium, pp. 5293-5295, Jul. 2005.

[2] *M. Nolan, D. R. Fatland, and L. Hinzman,* "DInSAR Measurement of Soil Moisture," IEEE Transactions on Geoscience and Remote Sensing, Vol. 41, No. 12, pp. 2802-2813, Dec. 2003.

[3] *O. Mora, R. Arbiol, V. Palà, A. Adell, and M. Torre*, "Generation of Accurate DEMs Using DInSAR Methodology (TopoDInSAR)", IEEE Geoscience and Remote Sensing Letters, Vol. 3, No. 4, Oct. 2006.

[4] *J.-L. Froger, F. Yukushima, P. Tinard, V. Cayol, T. Souriot, O. Mora, T. Staudacher, P. Durand, B. Fruneau, and N. Villeneuve*, "Multi Sensors InSAR Monitoring of Volcanic Activity: the February and April 2007 Eruptions at Piton de la Fournaise, Reunion Island, Imaged with ENVISAT-ASAR and ALOS-PALSAR Data", Fringe Workshop, Frascati, Italy, 26-30 Nov. 2007.

[5] *M. Chini, S. Atzori, E. Trasatti, C. Bignami, C. Kyriakopoulos, C. Tolomei, and S. Stramondo*, "The May 12, 2008 (Mw 7.9) Sichuan Earthquake (China): Multiframe ALOS-PALSAR DInSAR Analysis of Coseismic Deformation", IEEE Geoscience and Remote Sensing Letters, Vol. 7, No. 2, pp. 266-270, 2009.

[6] *Y. Luo, J. Zhang, Q. Zeng, J. Wu, L. Gong, W. Jiang, Y. Dai*, PS InSAR Monitoring of Land Subsidence in Suzhou", Beijing, ESA SP-655, 2008.

[7] *H. A. Zebker, and J. Villasenor,* "Decorrelation in Interferometric Radar Echoes", IEEE Transactions on Geoscience and Remote Sensing, Vol. 30, No. 5, pp. 950-959, Sept. 1992.

[8] *L. Zhang, X. Ding, and Z. Lu,* "Modeling PSInSAR Time Series Without Phase Unwrapping", IEEE Trans. on Geoscience and Remote Sensing, Vol. 49, No. 1, pp. 547-556, Jan. 2011.

[9] F. *Argenti, A. Lapini, T. Bianchi, L. Alparone*, " A tutorial on speckle reduction in synthetic aperture radar images," IEEE Geoscience and Remote Sensing Magazine, Vol. 1, No. 3, pp. 6–35, Sept 2013.

[10] *A. Ferretti, A. Fumagalli, F. Novali, C. Prati, F. Rocca, A. Rucci*, "A new algorithm for processing interferometric data-stacks: SqueeSAR," IEEE Transactions on Geoscience and Remote Sensing, Vol. 49, Nr. 9, pp. 3460-3470, Sept 2011.

[11] *A. Ferretti, C. Prati, F. Rocca*, "Nonlinear subsidence rate estimation using permanent scatterers in differential SAR interferometry," IEEE Transactions on Geoscience and Remote Sensing, Vol. 38, Nr. 5, pp. 2202-2212, Sept 2000.

[12] *A. Ferretti, C. Prati, F. Rocca,* "Permanent scatterers in SAR interferometry," IEEE Transactions on Geoscience and Remote Sensing, Vol. 39, Nr. 1, pp. 8-20, Jan 2001.

[13] *L C. Colesanti, A. Ferretti, F. Novali, C. Prati, and F. Rocca,* "SAR Monitoring of Progressive and Seasonal Ground Deformation using the Permanent Scatterer Technique," IEEE Trans. on Geoscience and Remote Sensing, Vol. 41, No. 7, pp. 1685-1701, Sept 2000.

[14] *R. Lanari, F. Casu, M. Manzo, G. Zeni, P. Bernardino, M. Manunta, A. Pepe,* "An overview of the small baseline subset algorithm: A DInSAR technique for surface deformation analysis," Pure and Applied Geophysics, Vol. 164, Nr. 4, pp. 637-661, 2007

[15] *G.H. Golub, and C.F. Van Loan*, "A New Algorithm for Surface Deformation Monitoring Based on Small Baseline Differential SAR Interferograms", IEEE Transactions on Geoscience and Remote Sensing, Vol. 40, No. 11, pp. 2375-2383, Nov. 2002.

[16] *J.S. Lee, K. Papathanassiou, T. Ainsworth, M. Grunes, A. Reigber*, "A new technique for noise filtering of SAR interferometric phase images," IEEE Transactions on Geoscience and Remote Sensing, Vol. 36, Nr. 5, pp. 1456-1465, Sep 1998

[17] *R. Touzi, A. Lopes, J. Bruniquel, P. Vachon*, "Coherence estimation for SAR imagery," IEEE Transactions on Geoscience and Remote Sensing, Vol. 37, No. 1, pp. 135-149, Jan 1999

[18] *A.N. Pettitt*, "A two-sample Anderson-Darling rank statistic," Biometrika, Vol. 63, No. 1, 1976

[19] Advanced Studies and Research Center, www.asrc.ro